

Article

# Sol-Gel Obtaining of TiO<sub>2</sub>/TeO<sub>2</sub> Nanopowders with Biocidal and Environmental Applications

Albena Bachvarova-Nedelcheva <sup>1,\*</sup>, Reni Iordanova <sup>1</sup>, Anton Naydenov <sup>1</sup>, Angelina Stoyanova <sup>2</sup>, Nelly Georgieva <sup>3</sup>, Veronica Nemska <sup>3</sup> and Tsvetelina Foteva <sup>3</sup>

<sup>1</sup> Institute of General and Inorganic Chemistry, Bulgarian Academy of Sciences, Acad. G. Bonchev Str., bld. 11, 1113 Sofia, Bulgaria

<sup>2</sup> Department Chemistry and Biochemistry, Faculty of Pharmacy, Medical University-Pleven, Kl. Ohridski Str., 1, 5800 Pleven, Bulgaria

<sup>3</sup> Department Biotechnology, Faculty of Chemical and Systems Engineering, University of Chemical Technology and Metallurgy, Kl. Ohridski Blvd, 8, 1756 Sofia, Bulgaria

\* Correspondence: albenadb@svr.igic.bas.bg

**Abstract:** TiO<sub>2</sub>/TeO<sub>2</sub> powders were obtained by an aqueous sol-gel method. Telluric acid (H<sub>6</sub>TeO<sub>6</sub>) and titanium butoxide were used as precursors. The as-prepared gel was step-wisely heated in the temperature range 200–700 °C and subsequently characterized by XRD, IR, and UV-Vis analysis and SEM. Mixtures containing TiO<sub>2</sub> (anatase), α-TeO<sub>2</sub> (paratellurite), and TiTe<sub>3</sub>O<sub>8</sub> were established by XRD as final products, depending on heating temperature. The thermal stability of the obtained gels in the temperature range 100–400 °C was investigated. It was found by IR spectroscopy that the samples heated up to 300–400 °C consist mainly of an organic–inorganic amorphous phase which is transformed into an inorganic one above these temperatures. The microstructure of the gels was verified by scanning electron microscopy (SEM). The photocatalytic degradation of the synthesized nanopowders toward Malachite green organic dye (MG) was examined in order to evaluate the potential applications for environmental remediation. The prepared TiO<sub>2</sub>/TeO<sub>2</sub> samples showed up to 60% decoloration efficiency after 120 min exposure to UV-light. The composition exhibited good antimicrobial activity against *E. coli* K12. The properties of the obtained material were investigated by the reactions of complete catalytic oxidation of different alkanes and toluene, and it could be suggested that TiO<sub>2</sub>/TeO<sub>2</sub> powders are promising material for use as an active phase in environmental catalysts.

**Keywords:** sol-gel; powders; antibacterial properties; photocatalytic properties



**Citation:** Bachvarova-Nedelcheva, A.; Iordanova, R.; Naydenov, A.; Stoyanova, A.; Georgieva, N.; Nemska, V.; Foteva, T. Sol-Gel Obtaining of TiO<sub>2</sub>/TeO<sub>2</sub> Nanopowders with Biocidal and Environmental Applications.

*Catalysts* **2023**, *13*, 257. <https://doi.org/10.3390/catal13020257>

Academic Editor: Jae Sung Lee

Received: 30 November 2022

Revised: 12 January 2023

Accepted: 17 January 2023

Published: 22 January 2023



**Copyright:** © 2023 by the authors. Licensee MDPI, Basel, Switzerland. This article is an open access article distributed under the terms and conditions of the Creative Commons Attribution (CC BY) license (<https://creativecommons.org/licenses/by/4.0/>).

## 1. Introduction

Titania (TiO<sub>2</sub>) is one of the most popular materials for (photo)catalytic applications and solar energy conversion. Its wide use for environmental remediation is due to the excellent properties such as non-toxicity, stability, and low cost. A number of excellent review papers devoted to various aspects of TiO<sub>2</sub> have been published [1–7]. The low temperature sol-gel method is widely used for production of TiO<sub>2</sub> nanoparticles with large surface area [8]. It is also known that due to nontoxicity, long-term photostability, and high effectiveness, TiO<sub>2</sub> has been widely utilized in mineralizing toxic and nonbiodegradable environmental contaminants [9]. TiO<sub>2</sub> also possesses good mechanical resistance as well as stability in acidic and oxidative environments. These properties make TiO<sub>2</sub> a desirable candidate for heterogeneous catalyst support [10].

The unceasing attention of scientists to the photocatalysis with metaloxide-based semiconductors is due to their ability for reducing the toxic substances and removal of heavy organic contaminants from wastewater [1,9,10]. The literature data revealed that the photocatalytic degradation to purify water is considered an effective and economical technique [1,9,11]. Among the various available metal oxides, TiO<sub>2</sub> is the preferable one as

a prominent candidate for antibacterial and photocatalysis activity. Nowadays, new active photocatalysts have been obtained for Methylene blue and Oxytetracycline degradation under dark and visible light conditions [12,13]. Photocatalytic reactions at the surface of titanium dioxide have been attracting much attention in view of their practical applications to environmental cleaning such as self-cleaning of tiles, glasses, and windows [14]. As it is known  $\text{TiO}_2$  absorbs only near-ultraviolet (UV) light and the doping with metal ions has been investigated to extend its absorption to the visible light region for better photocatalytic performance. The photocatalytic activity of metal-doped  $\text{TiO}_2$  is determined by the type of dopant. It was reported that metal ion dopants strongly modify the anatase-rutile phase transition temperature, change the photoreactivity of  $\text{TiO}_2$  nanosized particles, and enhance the catalytic properties of supported metals or oxides. Various methods for synthesis such as a hydrothermal route, sol-gel route, and wet impregnation have been studied for doped  $\text{TiO}_2$  powders. Among them, the sol-gel process is the most widely used approach consisting of two steps: hydrolysis of a titanium salt and a further condensation reaction. It was found that this method leads to obtaining the greatest homogeneous distribution of the dopant in the host matrix and a high surface area of as-prepared  $\text{TiO}_2$  particles [15].  $\text{TiO}_2$  shows relatively high reactivity and chemical stability under ultraviolet light ( $\lambda < 387 \text{ nm}$ ), and its energy exceeds the band gap of 3.3 eV in the anatase crystalline phase [14].

Malachite Green (MG), a triphenylmethane dye, is a compound that is mainly used in textile industries and partly used in aquaculture in fungicides and ectoparasiticides [16–18]. Several review papers concerning the wide range of toxicological effects of malachite green (MG) and its effect on the ecosystem have been published [19]. It has been generalized that the toxicity of this dye increases with exposure time, temperature, and concentration.

Additionally,  $\text{TiO}_2$  NPs can be used as an antibacterial agent because of strong oxidation activity and superhydrophilicity. Specifically, their antimicrobial activity is greatly dependent on the photocatalytic performance of  $\text{TiO}_2$ , which depends strongly on its morphological, structural, and textural properties and these peculiarities have been described in details in several review papers and book chapters [20–23]. In recent years there has been an increase in the resistance of several bacterial strains to these substances, and therefore there is currently a great interest in the search for new antimicrobial substances. With this in mind, titanium dioxide nanoparticles are one of the antimicrobial NPs whose study still continues to gain interest. It is important to highlight that some research works have evidenced increased antimicrobial activity of  $\text{TiO}_2$  NPs after irradiation with UV-A light due to the photocatalytic nature of this oxide. The mechanism referring to the antimicrobial action of  $\text{TiO}_2$  is commonly associated to reactive oxygen species (ROS) which affect and destroy the bacterial cells by different mechanisms [24].

As a conditional network former,  $\text{TeO}_2$  does not form glass alone, but tellurite glasses are attractive because of their excellent optical properties (high refractive index, high third order nonlinear properties, wide optical window from the ultraviolet to the infrared region, etc.) [25]. The sol-gel method is an alternative way to extend the application of new tellurite compositions. Powders and films in the  $\text{TiO}_2\text{-TeO}_2$  and  $\text{TeO}_2\text{-PbO-TiO}_2$  systems have been reported in several papers, irrespective of the anomalously high hydrolysis rate of  $\text{Te(VI)}$ .

Nowadays, the most popular research field is designing of new nanomaterials using metal oxides with dual applications (photocatalyst and antibacterial agent). The nanocomposite potential's is due to their ease of synthesis, size, shape, and doping with countless metal and non-metal materials with different concentration which made them suitable to enhance the properties of existing material [10,26].

Our team has extensive experience in the sol-gel obtaining of composite powders containing  $\text{TiO}_2$ . Until now, we have obtained different binary, ternary, and multicomponent composites with good photocatalytic and antibacterial properties applying this technique [27–31]. This research is a continuation of our previous investigations on the sol-gel obtaining of  $\text{TiO}_2$  nanocomposite powders by applying  $\text{Te(VI)}$  acid and Ti butoxide as a new combination of precursors. We continue searching for new combinations

of compositions which have not previously been investigated with the focus on those with improved photocatalytic and antibacterial properties. To our knowledge, there are no reported data on TiO<sub>2</sub>/TeO<sub>2</sub> sol-gel derived powders and study of their biocidal and environmental applications which emphasizes the novelty in the current work.

Progressing our studies, the aim of the present work is to synthesize TiO<sub>2</sub>/TeO<sub>2</sub> composite by sol-gel technique and to investigate its thermal, structural, and optical properties. The investigation has been also focused on the antibacterial and photocatalytic properties of the as-prepared composition. Additionally, its catalytic properties for neutralization of waste gases containing VOCs were evaluated applying Pd.

## 2. Results and Discussion

### 2.1. Phase Transformations and Thermal Stability of the Gel

The XRD patterns of as-prepared TiO<sub>2</sub>/TeO<sub>2</sub> sample heat treated from 200 to 700 °C are shown in Figure 1. The metallic tellurium (JCPDS 78-2312) is found predominantly up to 400 °C. At 400 °C it was registered that TiO<sub>2</sub> (anatase, JCPDS 78-2486) coexisted with metallic tellurium. With increasing the temperature (500 and 600 °C), the anatase became a dominant phase, while at 700 °C formation of crystalline TiTe<sub>3</sub>O<sub>8</sub> phase (JCPDS 50-0250) along with TiO<sub>2</sub> (rutile) were observed. The average crystallite size of the particles, calculated from the broadening of the diffraction line using Sherrer's equation is about 60 nm. Irrespective of using a different precursor (Te(VI) acid) in the performed experiment, the obtained XRD data are very similar to those obtained by other teams [32–34].

The specific surface area (SSA) results utilizing Brunauer–Emmett–Teller (BET) nitrogen adsorption experiments showed that SSA for the TiO<sub>2</sub>/TeO<sub>2</sub> sample was higher and had a value of 86 m<sup>2</sup>/g, while it dropped to 71 m<sup>2</sup>/g when the Pd was added.

DTA/TG curves of the as-prepared gel are presented in Figure 2. An endothermic effect appeared about 105 °C, which is attributed to the evaporation of organic solvent and desorption of physically adsorbed water. The observed weight loss is about 7%. Two broad exothermic peaks were registered at about 235 and 285 °C. The first one is related to the beginning of the decomposition of the organic groups (weight loss is ~8%) as in the pure TBT [35,36]. The second exothermic effect appeared at slightly higher temperature (285 °C) with around 15% weight loss, which suggests strong combustion of the organic components [37]. The noticed increase in the curve intensity about 400 °C suggests the presence of an exothermic effect due to the oxidation of Te to TeO<sub>2</sub>. For comparison, other authors established that this oxidation proceeded at similar temperatures [32,38,39].

### 2.2. IR and UV-Vis DRS Characterization

The phase transformations during the heat treatment were also studied by means of IR spectroscopy which is a more sensitive method, and the IR spectra are shown in Figure 3. The assignment of the bands is made on the basis of the literature data as well as our previous investigations [40–42]. At low temperature (200 °C), intensive characteristic bands in the range 1460–880 cm<sup>-1</sup> were observed. Generally, bands located between 1500–1300 cm<sup>-1</sup> assigned to the bending vibrations of CH<sub>3</sub> and CH<sub>2</sub> groups [43,44]. The band at 1120 cm<sup>-1</sup> is characteristic for the stretching vibrations of Ti-O-C, while those at 1080 and 1040 cm<sup>-1</sup> are assigned to the vibrations of terminal and bridging C-O bonds in butoxy ligands. For the ethylene glycol the asymmetric and symmetric stretching vibrations of C-O bonds in CH<sub>2</sub>-OH group are also at 1080 and 1040 cm<sup>-1</sup>. In the absorption range below 1000 cm<sup>-1</sup> there is an overlapping between the vibrations of different structural units TiO<sub>6</sub> and TeO<sub>n</sub> and their assignments are difficult to be made because one and the same band could be related to the vibrations of different structural units. We can assume that the band centered about 790 cm<sup>-1</sup> could be connected to the deformation vibrations of Ti-O-C bonds from butoxy groups [43,44]. On the other hand, bands in the range of 600–400 cm<sup>-1</sup> could be also related to the vibrations of TiO<sub>6</sub> building units [45]. Additionally, the typical vibrations of TeO<sub>4</sub> groups building up the crystalline TeO<sub>2</sub> are situated about 770, 660, and 640–630 cm<sup>-1</sup> [46–49].

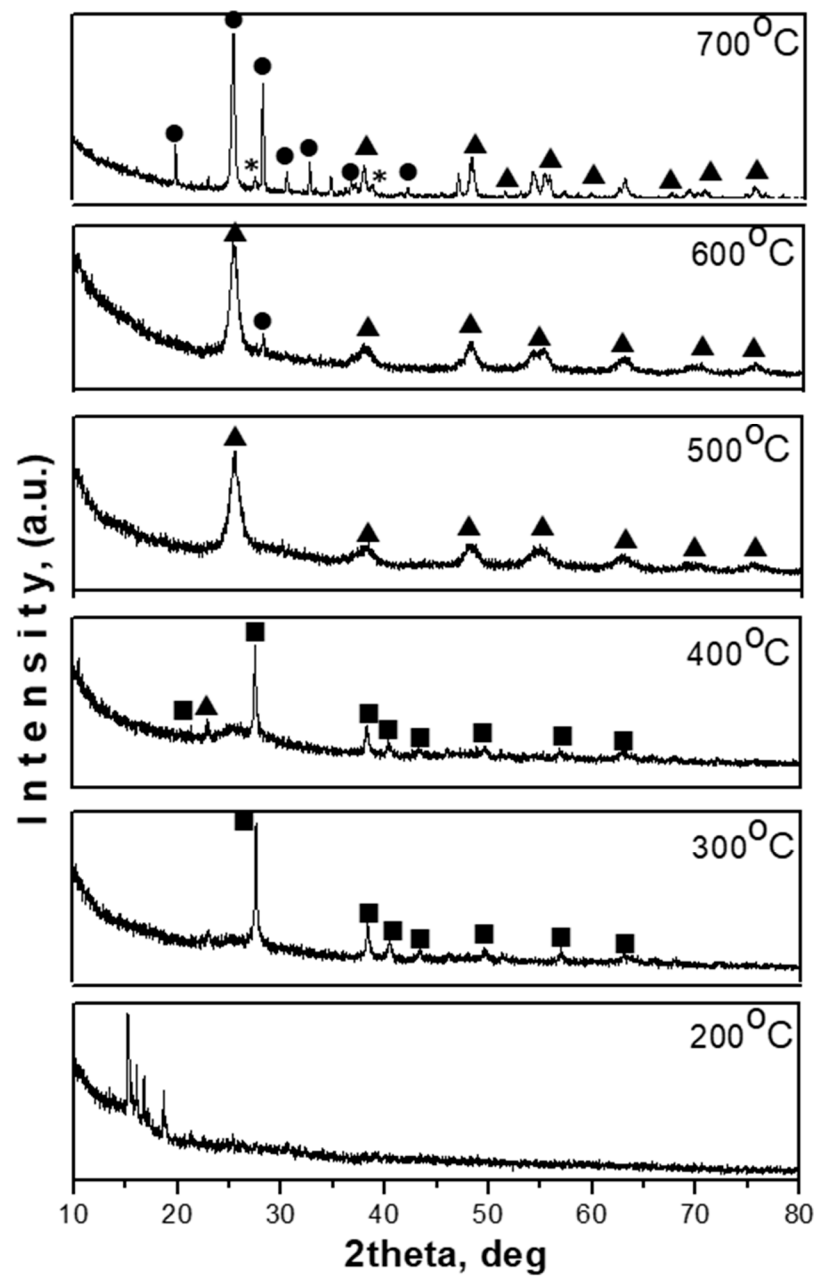


**Figure 1.** XRD patterns of sample with nominal composition 90TiO<sub>2</sub>.10TeO<sub>2</sub> heat treated at different temperatures: (■) Te, (▲) TiO<sub>2</sub>-anatase, (\*) TiO<sub>2</sub>-rutile, (●) TiTe<sub>3</sub>O<sub>8</sub>.

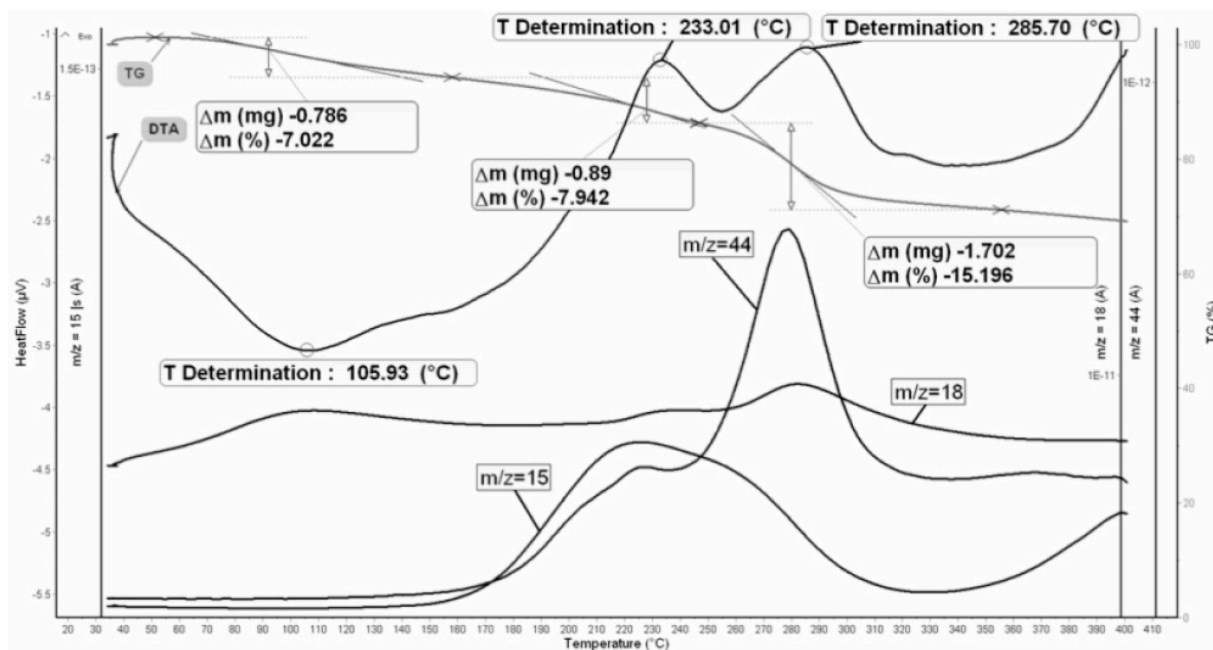


Figure 2. DTA/TG curves 90TiO<sub>2</sub>.10TeO<sub>2</sub> gel.

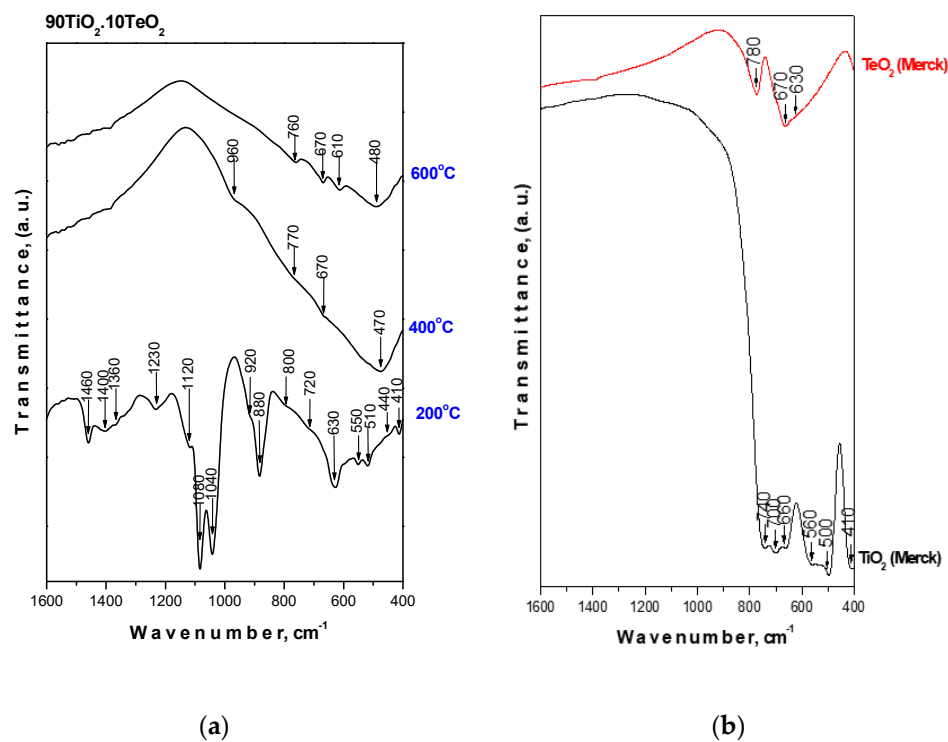


Figure 3. IR spectra of: (a) investigated sample heat treated at different temperatures and (b) TeO<sub>2</sub> and TiO<sub>2</sub> commercial products.

The bands above 1000 cm<sup>-1</sup>, characteristic of the organic groups, are not visible above 400 °C. The spectra at 400 and 600 °C are characterized mainly by bands below 900 cm<sup>-1</sup>, typical for the inorganic units (TiO<sub>6</sub> and TeO<sub>4</sub> units). These bands are broadened, with the low intensity that is a peculiarity of disordered systems. At these temperatures the overlapping between these vibrations makes difficulties for the IR assignment. The structural data are in good accordance with the XRD data.

The UV–visible analysis is considered a non-destructive and it is a powerful tool for exploring the optical features of nanocomposite powders [10]. Numerous factors influence the absorbance, such as surface, impurity centers, oxygen deficiency, and bandgap [10]. The optical absorption spectra of both gels  $90\text{TiO}_2 \cdot 10\text{TeO}_2$  and Ti(IV) butoxide were shown in Figure 4. The absorption edge and optical band gap values of the samples are summarized in Table 1. The UV-Vis spectra exhibit two maxima 240–260 nm and 320–340 nm which could be assigned to the isolated  $\text{TiO}_4$  and  $\text{TiO}_6$  units, respectively [50]. As it seen from the figure, for TBT gel, the intensity of UV peaks in the spectra at 240 nm and that near 320 nm are compatible which is an indication of the compatible amount of  $\text{TiO}_4$  and  $\text{TiO}_6$  polyhedra in the gel network. In the  $90\text{TiO}_2 \cdot 10\text{TeO}_2$  gel the peak at 340 nm is dominant which is a result of additional activation of hydrolysis-condensation processes [50]. The other peculiarity is the red shift of the absorption edges in the spectra. These observations are consistent with the reports in the literature for Te— and C—modified  $\text{TiO}_2$  compositions [51,52]. It was reported that [53] the doping of elementary Te into  $\text{TiO}_2$  induced an increase in absorption due to smaller band gap of Te than that of  $\text{TiO}_2$  (0.3 vs 3.2 eV). The UV-Vis spectra were also used to determine the optical band gap ( $E_{\text{opt}}$ ) of investigated sample (Table 1). The obtained data are corroborated by the literature data [54].

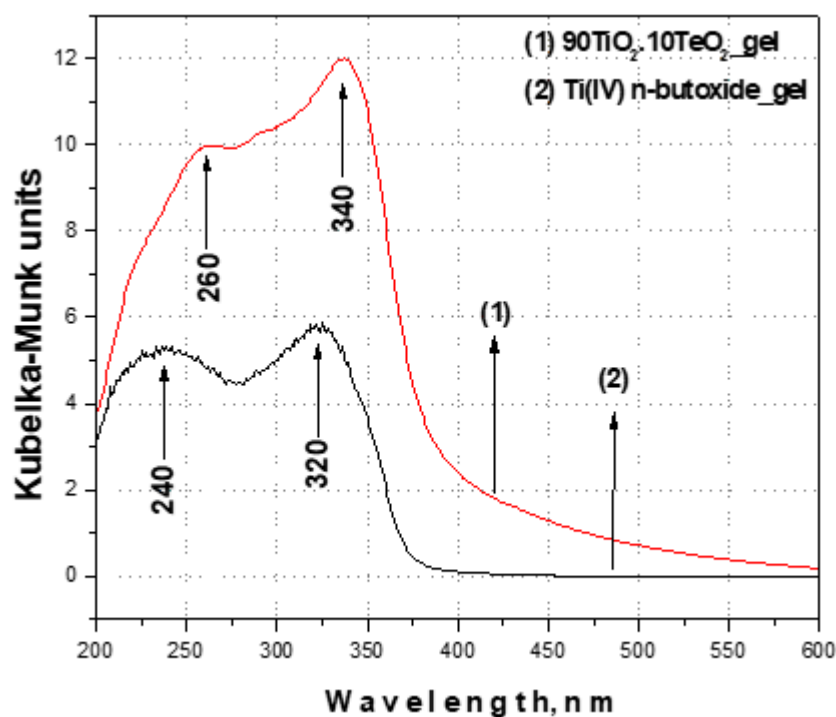


Figure 4. UV-Vis spectra of sample  $90\text{TiO}_2 \cdot 10\text{TeO}_2$  compared with Ti(IV) butoxide.

Table 1. Investigated  $\text{TiO}_2/\text{TeO}_2$  gel, observed cut-off and calculated optical band gap values ( $E_g$ ).

-	Sample	Cut-Off, nm	$E_g$ , eV
1.	Ti(IV) butoxide	375	3.31
2.	$90\text{TiO}_2 \cdot 10\text{TeO}_2$	395	3.14

### 2.3. Transmission Electron Microscopy

The HRTEM images performed in different parts of investigated samples  $90\text{TiO}_2/10\text{TeO}_2$  and  $90\text{TiO}_2/10\text{TeO}_2/\text{Pd}$  are shown in Figures 5–7. Predominantly spherical and well-shaped particles are observed with size between 50 nm to 100 nm, which corresponds to the results obtained by XRD. Bright field TEM micrographs from selected areas of the samples are shown in Figure 6. The composition map via STEM—XEDS analysis was

carried out to examine the distribution of elements in the composite sample. The results of mapping studies (Figures 5–7) portray the coexistence of Ti, O, Te, and Pd elements and their homogeneous distribution. These results demonstrated also that Pd was uniformly doped in the TiO<sub>2</sub> nanoparticles and did not contain segregated particles. The obtained data from the qualitative elemental analysis performed in different points of the sample surface are summarized in Table 2.

**Table 2.** Elemental analysis according to TEM.

Sample	Map Sum Spectrum	wt %
90TiO <sub>2</sub> /10TeO <sub>2</sub>	Ti	51.09
	O	33.95
	Te	14.96
90TiO <sub>2</sub> /10TeO <sub>2</sub> /Pd	Ti	57.78
	O	22.08
	Te	18.84
	Pd	1.5

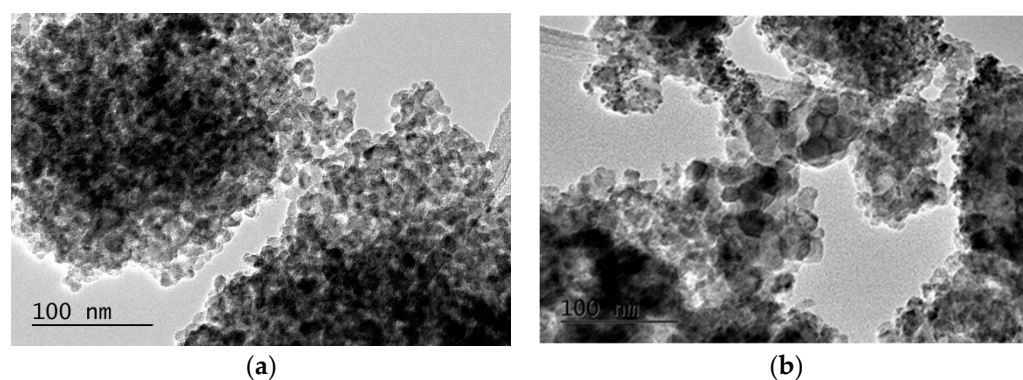


**Figure 5.** Bright field TEM micrographs from selected areas of samples 90TiO<sub>2</sub>/10TeO<sub>2</sub> heat treated at 600 °C (a) and 90TiO<sub>2</sub>/10TeO<sub>2</sub>/Pd (b).

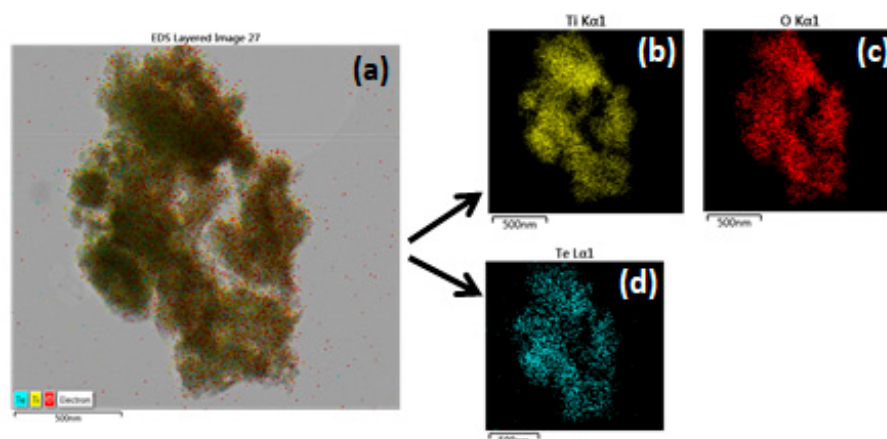


**Figure 6.** (a) Integral XEDS-STEM composition map from selected area of sample 90TiO<sub>2</sub>/10TeO<sub>2</sub> heat treated at 600 °C; (b) composition map of Ti; (c) composition map of O; (d) composition map of Te.

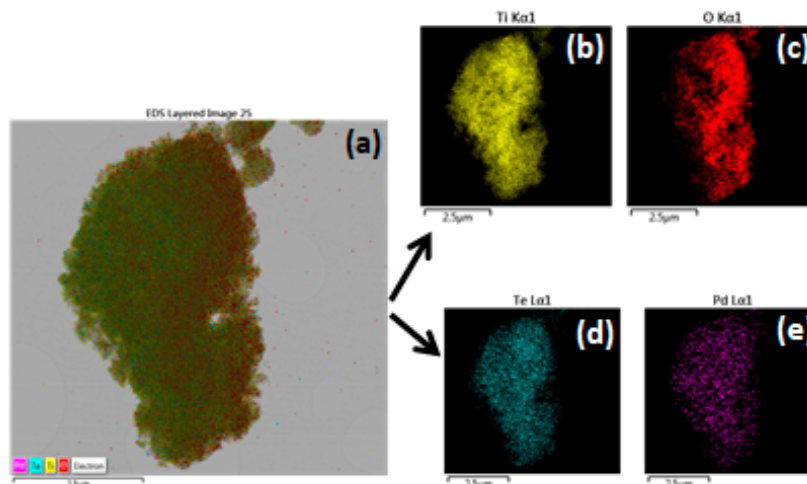


**Figure 7.** (a) Integral XEDS-STEM composition map from selected area of sample  $90\text{TiO}_2/10\text{TeO}_2/\text{Pd}$  heat treated at  $600\text{ }^\circ\text{C}$ ; (b) composition map of Ti; (c) composition map of O; (d) composition map of Te; (e) composition map of Pd.

#### 2.4. Antibacterial Assessment

The investigated  $90\text{TiO}_2.10\text{TeO}_2$  sample heat treated at  $200$  and  $400\text{ }^\circ\text{C}$  has been tested for antibacterial activity against *E. coli* K12 NBIMCC 407 (Figure 8). The testing has been performed by monitoring the cell reduction in their presence in a liquid medium and measuring the inhibition zones formed around the materials (Figure 8a,b).

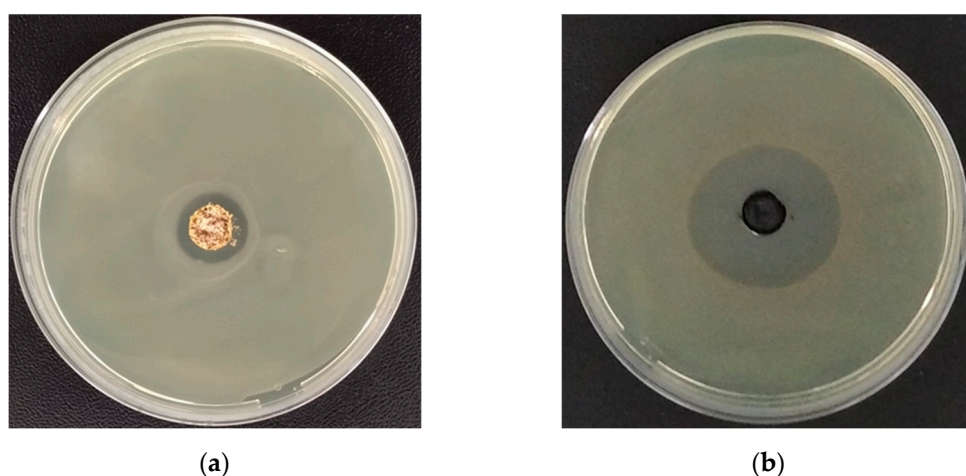


**Figure 8.** Antibacterial test result of the sample  $90\text{TiO}_2.10\text{TeO}_2$ : (a) heat treated at  $200\text{ }^\circ\text{C}$  and (b)  $400\text{ }^\circ\text{C}$  against *E. coli* K12 407.

Both tested powdered materials showed good antibacterial activity against *E. coli* K12 NBIMCC 407. However, the highest level of bacterial cell reduction was achieved by the sample heated at  $400\text{ }^\circ\text{C}$ —68% reduction (Figure 8b). The other sample, heat treated at  $200\text{ }^\circ\text{C}$  showed weaker antibacterial activity—50%. Obviously, the temperature of the heat treatment does not greatly affect the antibacterial behavior of materials. Additionally, the antibacterial properties of the tested materials were estimated by second microbiological method refers to the measurement of the zones, free of bacterial growth. The obtained results revealed well-formed inhibition zones around both materials. Lower antibacterial activity was observed again by sample heated at the lower temperature ( $200\text{ }^\circ\text{C}$ ) (inhibition zone = 16 mm) (Figure 8a).

In interpretation of the obtained data, it must be underlined that there are many factors influencing the antimicrobial activity of the synthesized  $\text{TiO}_2$  nanoparticles: morphology,

crystal nature, size, and specific surface area [20,55,56]. Some authors [20] summarize that the enhancement of the specific surface area stimulates the antimicrobial reduction in TiO<sub>2</sub> nanoparticles. This could be explained by the nature of titanium dioxide, and one of the main mechanisms of its action is through the generation of reactive oxygen species (ROS) on its surface during the process of photocatalysis when it is exposed to light at an appropriate wavelength. During this process free radicals were produced that contribute to the biocidal activity of the samples by destruction of cellular organic compounds [57]. On the other hand, the antimicrobial activity of TiO<sub>2</sub> even in the absence of photo activation has been also reported [57]. It has been found that an electromagnetic attraction between microorganisms and the TiO<sub>2</sub> NPs occurred due to the positive charge carried by the TiO<sub>2</sub> and the negative charges carried by the microorganisms' surface which leads to oxidation reactions. In this way TiO<sub>2</sub> deactivates cellular enzymes and DNA by coordinating to electron-donating groups, such as: thiols, amides, carbohydrates, indoles, and hydroxylys. The resulting pits formed in bacterial cell walls lead to increased permeability and cell death [57].

Analyzing our results, it could be generalized that the samples heated at higher temperature (400 °C) showed better antibacterial activity (68%) compared to those heated at 200 °C (50%). Our suggestion is that these results could be explained bearing in mind the XRD results (Figure 1), where the presence of elemental tellurium at a higher temperature and metal-organic complexes at 200 °C were established. It has been reported that when metal nanoparticles and organics are present in the antibacterial agent, the release of their ions retards the Gram-negative bacteria [20,58]. On the other hand, the relatively good antibacterial activity at both temperatures could be related to the lower bandgap (3.14 eV) as well as the higher surface area (86 m<sup>2</sup>/g) which contribute to the formation of highly reactive oxygen species (ROS) responsible for bacterial cell damage.

### 2.5. Photocatalytic Activity

The photocatalytic degradation of MG under UV irradiation has been tested in the presence of investigated 90TiO<sub>2</sub>.10TeO<sub>2</sub> sample. The photocatalytic properties were compared to those of TiO<sub>2</sub> obtained from Ti(IV) butoxide and to commercial TiO<sub>2</sub> (Fluka), used as a reference (Figure 9a). As can be seen from the figure, the best photocatalytic activity showed commercial pure TiO<sub>2</sub> (Fluka). The results of the photocatalytic test reveal that the addition of tellurium oxide did not improve the degradation of the MG dye at our experimental conditions and its effectiveness is comparable to those of TiO<sub>2</sub> obtained from Ti(IV) butoxide. These findings were confirmed by the application of pseudo-first-order kinetic model [59,60] for determination of the photodegradation rate constants in the degradation process of MG, commonly expressed by the equation:

$$\ln C_0/C_t = kt,$$

where  $k$  is the photodegradation rate constant (min<sup>-1</sup>),  $C_0$  is the initial concentration and  $C_t$  is the concentration at any time,  $t$ .

Semi-logarithmic plots of the concentration data gave straight lines, from which slopes the rate constants are derived (Figure 9b). The rate constants of synthesized TiO<sub>2</sub>/TeO<sub>2</sub> sample, pure TiO<sub>2</sub> and the commercial TiO<sub>2</sub> are 0.0072, 0.0065, and 0.0674 min<sup>-1</sup>, respectively. All correlation coefficients ( $R^2$ ) were higher than 0.947. As it is also seen from the figure, the best photocatalytic activity showed commercial pure TiO<sub>2</sub> (Fluka) with 100% decoloration efficiency after 60 min irradiation. The photodegradation efficiency of the TiO<sub>2</sub>/TeO<sub>2</sub> sample was similar to that of synthesized from Ti(IV) butoxide pure TiO<sub>2</sub>—both achieved only 35% bleaching after 60 min irradiation, and less than 60% after 120 min of illumination. It is well known that the photocatalytic activity of doped TiO<sub>2</sub> depends on many factors, such as synthesis method, dopant concentration, light source, particle size, and surface area. Obviously, at our experimental conditions, the presence of tellurium was not beneficial to the photoactivity under UV irradiation.

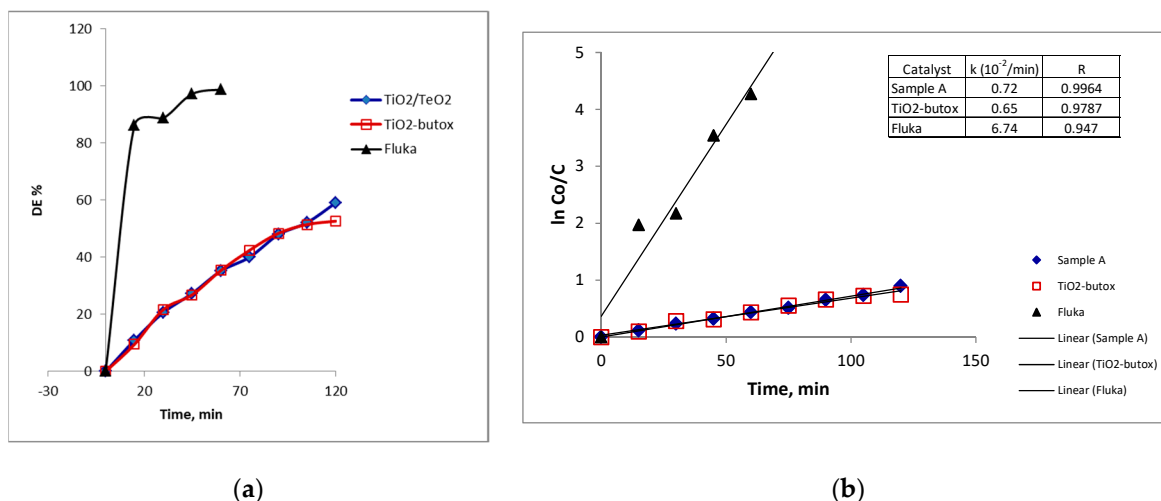


**Figure 9.** (a) Photodegradation efficiency of TiO<sub>2</sub>/TeO<sub>2</sub>, TiO<sub>2</sub>-butox and TiO<sub>2</sub>-Fluka samples in decoloration of MG under UV irradiation; (b) Photocatalytic reaction kinetics of MG decoloration by TiO<sub>2</sub>/TeO<sub>2</sub>, TiO<sub>2</sub>-butox and TiO<sub>2</sub>-Fluka samples.

Girish et al. [61] generalized that it is difficult to compare the photocatalytic activities of doped with metal ion titania. They also stated that there are conflicting results on the effects of doping on the photoactivity of TiO<sub>2</sub>. The wide variability of reports on the photoactivity of metal ion doped titania is due to the specific preparation methods, experimental conditions used, and the broad array of chemical reactions used to verify photoactivity over a range of wavelengths  $\lambda > 400$  nm. Fundamentally, these issues can be understood in terms of: (i) lack of surface structure facilitating surface transfer and reactivity of carriers and (ii) the distribution of dopant-induced localized states not being optimal to facilitate the photo-oxidation reactions.

However, there is no study comparing the biocidal activity and photocatalytic properties of TiO<sub>2</sub>/TeO<sub>2</sub> sample. In our investigations we observed different trends for photocatalytic and antibacterial activities. Although photocatalytic degradation and antibacterial activity are frequently attributed to the same mechanisms (reactive oxygen species (ROS) generation), it has been recently shown that they did not follow the same trends [60,62]. This phenomenon has been stated already in our previous paper concerning other systems containing TiO<sub>2</sub> [62]. The observed different trends could probably be explained by the direct oxidation/reduction processes occurring at the catalyst surface for the dye degradation while antibacterial activity may occur due to the involvement of ROS produced.

## 2.6. Catalytic Activity Test

The above-described properties of sol-gel derived 90TiO<sub>2</sub>.10TeO<sub>2</sub> offer the possibility to develop a thermally stable material with potential application in the environmental catalysis. In order to investigate this possibility, catalytic activity tests in the oxidation of CO and methane were performed. The modification of TiO<sub>2</sub> by Pd leads to remarkably high activity in the reaction of CO oxidation (Figure 10). At high gas hourly space velocity (GHSV = 46,150 h<sup>-1</sup>) and in the presence of 1 vol. % water vapor, the reaction begins at almost ambient temperatures (50 °C). For practical application it is of interest to predict the activity at gas hourly space velocities ranged at 15,000 h<sup>-1</sup>. The results, obtained by the mathematic modeling using the data at GHSV = 46,150 h<sup>-1</sup> and recalculated further to GHSV = 15,000 h<sup>-1</sup> are presented in Figure 11. Obviously, in the presence of water vapor one may achieve T<sub>90</sub> (temperature for conversion of 90%) conversion of CO at 120 °C, T<sub>50</sub> being 89 °C.

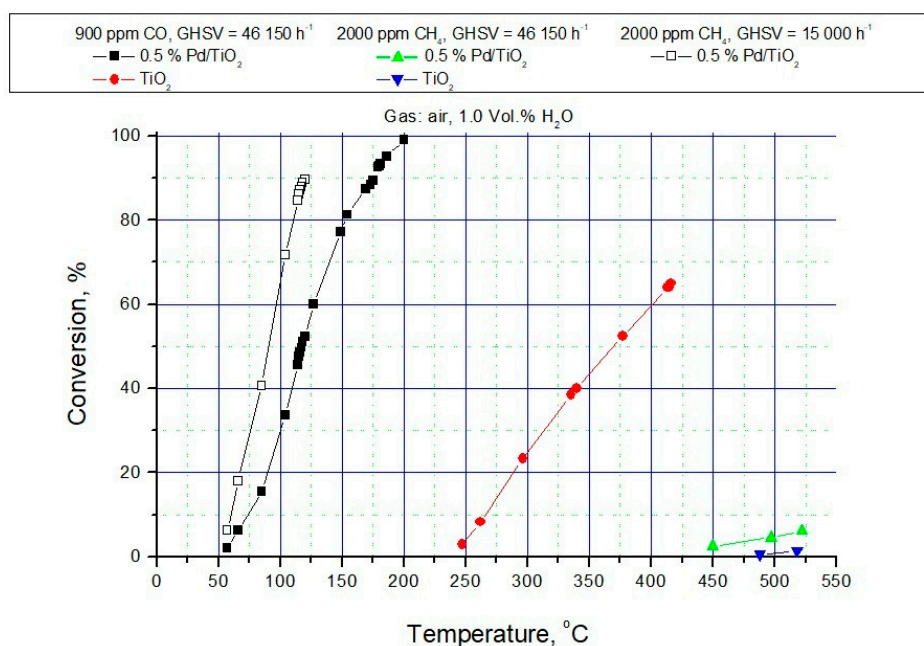


**Figure 10.** Temperature dependencies of the conversion during the catalytic oxidation of CO, methane over TiO<sub>2</sub> and TiO<sub>2</sub>/0.5 wt% Pd catalysts.

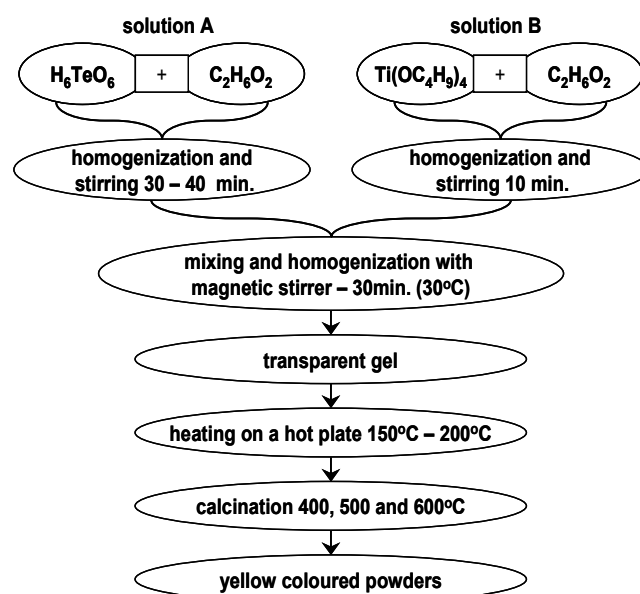


**Figure 11.** Scheme for the sol-gel synthesis of samples.

The activity towards methane combustion is relatively low, when compared with similar Pd-based catalysts; however, the use of TiO<sub>2</sub> as catalytic support increases the SO<sub>2</sub>—tolerance of the exhaust gas catalysts [63,64], due to the preferred sulfite formation on the catalytic surface, rather than the formation of the stable and difficult to remove sulfates.

### 3. Materials and Methods

#### 3.1. Samples Preparation

Based on our previous study on the gel formation in the binary TiO<sub>2</sub>-TeO<sub>2</sub> system, a composition containing 90 mol% TiO<sub>2</sub> was selected (90TiO<sub>2</sub>.10TeO<sub>2</sub>) and subjected to detailed investigations. Knowing that tellurium alkoxides possess a high hydrolysis rate [37,65–67] we used Te(VI) acid (H<sub>6</sub>TeO<sub>6</sub>, Sigma-Aldrich, Darmstadt, Germany) in a

combination of Ti(IV) butoxide (Fluka AG, Seelze, Germany) and ethylene glycol (C<sub>2</sub>H<sub>6</sub>O<sub>2</sub>) (99% Sigma-Aldrich, Darmstadt, Germany). The scheme for synthesis is presented in Figure 11. The initial solutions were prepared by dissolving the precursors in ethylene glycol by vigorous magnetic stirring while keeping the molar ratio T(IV) butoxide/C<sub>2</sub>H<sub>6</sub>O<sub>2</sub> = 1:1 and H<sub>6</sub>TeO<sub>6</sub>/C<sub>2</sub>H<sub>6</sub>O<sub>2</sub> = 1:2. Finally, both solutions were mixed with vigorous stirring. During the experimental procedure, no additional water was added. The sol-gel hydrolysis reaction was accomplished only in the presence of air moisture. By doing this, a transparent gel was obtained and followed by heat treatment at 200 °C in air in order to hydrolyze unreacted -OR groups as well as to decrease their content. Aiming to verify the phase and structural transformations, the gels were subjected to further stepwise heating from 300 to 700 °C. The calcination of the samples was performed for 2 h exposure time in air, until obtaining powder. The calcination temperature was selected on the basis of our previous investigations [68]. The pH during the experiments was measured at 7.5–8.0. The photocatalytic properties of the synthesized powders were compared with those of a commercial TiO<sub>2</sub> (Fluka AG, Seelze, Germany).

#### Pd Impregnation over 90TiO<sub>2</sub>/10TeO<sub>2</sub>

For verifying the catalytic properties, the so prepared 90TiO<sub>2</sub>/10TeO<sub>2</sub> powdered samples were modified by Pd (0.5 wt%) using the incipient wetness impregnation method. The impregnation was carried out at room temperature for 6 h using a solution of Pd(NO<sub>3</sub>)<sub>2</sub> (99.9%, Alfa Aesar, Kandel, Germany), drying at room temperature overnight and calcination at 500 °C for 2 h in argon atmosphere [69].

#### 3.2. Samples Characterization

Powder XRD patterns were registered at room temperature with a Bruker D8 Advance (Berlin, Germany) X-ray powder diffractometer with a Cu K $\alpha$  radiation ( $k = 1.54056 \text{ \AA}$ ) with a LynxEye solid position sensitive detector and X-ray tube operated at 40 kV and 40 mA. X-ray diffraction patterns were recorded in the range of 5.3–80° 2 $\theta$  with a step of 0.02° 2 $\theta$ . The decomposition process of the as prepared and aged in air gels was determined by differential thermal analysis (LABSYS<sup>TM</sup> EVO apparatus, Setaram, Lyon, France) with Pt-Pt/Rh thermocouple at a heating rate of 10 K/min in air flow, using Al<sub>2</sub>O<sub>3</sub> as a reference material. The accuracy of the temperature was  $\pm 5 \text{ }^\circ\text{C}$ . Heating of the samples was limited up to 600 °C. Gases evolved (EGA) during the thermal treatments were analyzed by mass spectrometry (MS) with a Pfeiffer OmniStar<sup>TM</sup> mass spectrometer (Pfeiffer Vacuum Technology AG, Wetzlar, Germany). Mass spectra recorded for samples A, C and D (Figure 3) show the  $m/z = 15, 18$  and  $44$  signals, being ascribed to CH<sub>3</sub>, H<sub>2</sub>O and CO<sub>2</sub>, respectively. The infrared spectra were registered in the range 1600–400 cm<sup>-1</sup> using the KBr pellet technique on a Nicolet-320 FTIR spectrometer (Madison, USA) with 64 scans and a resolution of  $\pm 1 \text{ cm}^{-1}$ . The optical absorption spectra of the powdered samples in the wavelength range 200–1000 nm were recorded by a UV–VIS diffused reflectance Spectrophotometer Evolution 300 (Thermo Electron Corporation, Madison, WI, USA) using a magnesium oxide reflectance standard as the baseline. The band gap energies ( $E_g$ ) of the samples were calculated by the Planck's equation:  $E_g = \frac{h \cdot c}{\lambda} = \frac{1240}{\lambda}$ , where  $E_g$  is the band gap energy (eV),  $h$  is the Planck's constant,  $c$  is the light velocity (m/s), and  $\lambda$  is the wavelength (nm). The morphology of the samples was examined by Transmission Electron Microscopy (TEM) investigations were performed on a JEOL JEM 2100 instrument (Tokyo, Japan) at an accelerating voltage of 200 kV. The specimens were prepared by grinding and dispersing them in ethanol by ultrasonic treatment for 6 min. The suspensions were dripped on standard carbon/Cu grids. Additional support for the existence of all participated elements in the investigated samples was performed by X-ray energy dispersive spectrometry (XEDS) elemental mapping studies. The specific surface areas (BETs) were determined by low-temperature (77.4 K) nitrogen adsorption in NOVA 1200e (Quantachrome Instruments NOVA 1200e apparatus, Anton Paar GmbH,

Graz, Austria) surface area and pore analyzer at relative pressures  $p/p_0 = 0.1\text{--}0.3$  using BET equation.

### 3.2.1. Photocatalytic Activity Experiments

The photocatalytic performance of the synthesized samples was evaluated by the extent of photodegradation of the organic dye Malachite green (MG) as a model pollutant. Reaction suspensions were prepared by adding 100 mg of synthesized photocatalysts to 150 mL MG water solution. For all experiments, the concentration of MG dye was 5 ppm.

Before irradiation, the suspensions were magnetically stirred and maintained for 30 min in the dark to attain the absorption–desorption equilibrium between the photocatalyst surface and dye molecules. Irradiation with UV-light was provided by a black light blue lamp (Sylvania BLB 50 Hz 8W T5) with the major fraction of irradiation occurring at 365 nm. The lamp was fixed 10 cm above the solution surface. Each MG/catalyst suspension has been exposed to UV-light with vigorous stirring. The zero timing was the moment of the UV lamp switch on. At specific time intervals, an aliquot (3 mL) of the suspension was extracted from the photoreacted mixture and centrifuged to remove the catalyst particles. At our experimental conditions the pH of the dye solution during the adsorption process varied in the range 5–6 and the pH values of supernatants after illumination were in the range 6–7. The progress of the gradual decomposition of dye was monitored by a Jenway 6505 UV-Vis spectrophotometer (designed and manufactured in UK) at the maximum absorption wavelength of MG—618 nm.

It is a fact that the absorption intensity is directly proportional to dye concentration. Thus, the percentage of degradation of dye was estimated using the following equation:

$$D\% = \frac{C_0 - C_t}{C_0} \times 100$$

where D denotes the percentage of photodegradation efficiency,  $C_0$  is the dye concentration at zero time and  $C_t$  is the concentration after the illumination time t.

### 3.2.2. Antimicrobial Assay

The antibacterial activity of the tested materials was investigated using *Escherichia coli* K12 NBIMCC 407 as a bacterial reference strain. It was obtained from the National Bank for Industrial Microorganisms and Cell Cultures (NBIMCC, Bulgaria) and cultivated in Luria-Bertani (LB) broth on a shaker-incubator ES-20/60 (Biosan, Riga, Latvia, 120 rpm) at 37 °C for 24 h. The first method of antimicrobial assay consists of the determination of antibacterial potential of the materials by studying the cell reduction after exposure to them. For this purpose, 100  $\mu\text{L}$  of the strain suspension ( $\text{OD}_{610} \text{ nm} = 1.9$ ) and 10 mg of each material were added to flasks, containing 100 mL LB broth. The control was a flask containing only bacterial cells (without materials added). After 24 h of incubation, 50  $\mu\text{L}$  of the culture broth of each flask was seeded on sterile LB agar plates. The number of colonies grown after 24-h incubation in an incubator (Binder, Germany) was used to calculate the percentage of cell reduction, according to Bachvarova-Nedelcheva et al. [56]. In addition, the antibacterial potential of the materials against the test strain was also determined by the agar-well diffusion method [70]. Sterile LB agar plates were inoculated with 100  $\mu\text{L}$  of an exponential culture of *E. coli* K12 NBIMCC 407, using the spread-plate method. A quantity of 100 mg of the materials was loaded onto marked wells, prepared in advance in the agar plates and were then cultured in an incubator at 37 °C for 24 h. The antibacterial activity was assessed by measuring the diameter of the obtained inhibition zones. All tests were performed in triplicate and the results obtained showed the mean values.

### 3.2.3. Catalytic Activity Tests

The following testing conditions were applied: catalyst bed volume of 0.5  $\text{cm}^3$ , irregular shaped particles having an average diameter of 0.7 mm, reactor diameter of 8.0 mm, and quartz glass ( $D_{\text{reactor}}/D_{\text{particles}} > 10$ ). The gas hourly space velocity (GHSV) was

fixed to  $46,150 \text{ h}^{-1}$ . For compensation of the adiabatic effect of the reaction, the catalyst bed temperature was kept almost constant (the deviation did not exceed  $\pm 1 \text{ }^\circ\text{C}$ ). The pressure drop was measured to be below 0.21 m water column. The axial dispersion effect was not subtracted since the catalyst bed is corresponding to a chain of more than 10 ideal-mixing cells along the reactor length. Therefore, the geometrical characteristics and the flow conditions in the catalytic reactor allow the consideration that the reactor is operating as isothermal plug flow reactor (PFR). The inlet concentrations of reactants were fixed as follows: methane concentrations at 2000 ppm; CO 900 ppm; and oxygen: 20.9 vol%. All gas mixtures were balanced to 100% with nitrogen (4.0 grade). The ability to reproduce the results and the confidence intervals for the measured conversion degree were the subject of preliminary tests on repeating the experimental runs under conditions similar (but not identical) for each experimental run represented in the study. The calculated value for the standard deviation ( $\pm 1.5\%$ ) was calculated on the basis of six measurements in each experimental point. The reported results are based on averaged values for the conversion degree within two parallel measurements. The gas analysis was performed by the using of mass spectrometer of the CATLAB system (Hiden Analytical), additionally supplemented by on-line gas-analyzers of CO/CO<sub>2</sub>/O<sub>2</sub> (Maihak) and THC-FID (total hydrocarbon content with a flame ionization detector, Horiba). The possible formation of oxidized organics by products was monitored by a GC-MS-analyzer, model Agilent AL7890A (Santa Clara, CA, USA).

#### 4. Conclusions

Aqueous sol-gel method was used for preparation of 90TiO<sub>2</sub>/10TeO<sub>2</sub> gel which was subjected to detailed investigations. It was established by XRD and IR analysis that the sample preserved the organic constituents up to 300 °C and the organic–inorganic amorphous phase transformed into inorganic one above 400 °C. The simultaneous existence of several crystalline phases TiO<sub>2</sub> (anatase),  $\alpha$ -TeO<sub>2</sub> and TiTe<sub>3</sub>O<sub>8</sub> were registered up to 700 °C. The UV–Vis spectroscopy showed two maxima about 240–260 nm and 320–340 nm related to the isolated TiO<sub>4</sub> units and condensed TiO<sub>6</sub> groups. The photocatalytic test reveals that the addition of tellurium oxide did not lead to better activity. The photodegradation efficiency of the TiO<sub>2</sub>/TeO<sub>2</sub> sample was similar to that of synthesized from Ti(IV) butoxide pure TiO<sub>2</sub>—both achieved only 35% bleaching after 60 min irradiation, and less than 60% after 120 min of illumination. The composition exhibited satisfactory antimicrobial activity against *E. coli* K12 as the samples heated at higher temperature (400 °C) showed better antibacterial activity (68%) compared to those heated at 200 °C (50%). The properties of the obtained material were investigated by the reactions of complete catalytic oxidation of different alkanes and toluene and it could be suggested that TiO<sub>2</sub>/TeO<sub>2</sub> powders can be considered as prospective material for use as an active phase in the preparation of environmental catalysts. The mathematical model simulations show that the industrial adiabatic reactor for 99% abatement of CO at gas flow of 10,000 Nm<sup>3</sup>/h should have the following dimensions: catalyst bed length 0.03 m; catalytic bed diameter 2.22 m (inlet temperature 118 °C; outlet temperature 126.7 °C). Therefore, further investigation is required to develop more efficiency of such powders aiming to improve their applications.

**Author Contributions:** Conceptualization, A.B.-N. and R.I.; methodology, A.B.-N. and R.I.; photocatalytic tests, A.S.; antibacterial properties N.G., V.N. and T.F.; catalytic tests, A.N.; writing—A.B.-N., A.S. and A.N.; supervision, R.I. and A.S. All authors have read and agreed to the published version of the manuscript.

**Funding:** This research received no external funding.

**Data Availability Statement:** The data presented in this study are available on request from the corresponding author.

**Acknowledgments:** This work was supported by the European Regional Development Fund within the Operational Programme “Science and Education for Smart Growth 2014–2020” under the Project CoE “National center of mechatronics and clean technologies” BG05M2OP001-1.001-0008. Research

equipment of distributed research infrastructure INFRAMAT supported by Bulgarian Ministry of Education and Science under contract D01-284/17.12.2019 was used.

**Conflicts of Interest:** The authors declare no conflict of interest.

## References

1. Carp, O.; Huisman, C.L.; Reller, A. Photoinduced reactivity of titanium dioxide. *Prog. Solid State Chem.* **2004**, *32*, 33–117. [[CrossRef](#)]
2. Fujishima, A.; Rao, T.N.; Tryk, D.A. Titanium dioxide photocatalysis. *J. Photochem. Photobiol. C Photochem. Rev.* **2000**, *1*, 1–21. [[CrossRef](#)]
3. Mor, G.K.; Varghese, O.K.; Paulose, M.; Shankar, K.; Grimes, C.A. A review on highly ordered, vertically oriented TiO<sub>2</sub> nanotube arrays: Fabrication, material properties, and solar energy applications. *Sol. Energy Mater. Sol. Cell* **2006**, *90*, 2011–2075. [[CrossRef](#)]
4. Chen, X.; Mao, S.S. Titanium dioxide nanomaterials: Synthesis, properties, modifications, and applications. *Chem. Rev.* **2007**, *107*, 2891–2959. [[CrossRef](#)] [[PubMed](#)]
5. Thompson, T.L.; Yates, J.T., Jr. Surface science studies of the photoactivation of TiO<sub>2</sub>—New photochemical processes. *Chem. Rev.* **2006**, *106*, 4428–4453. [[CrossRef](#)]
6. Diebold, U. The surface science of titanium dioxide. *Surf. Sci. Rep.* **2003**, *48*, 53–229. [[CrossRef](#)]
7. Linsebigler, A.L.; Lu, G.; Yates, J.T. Photocatalysis on TiO<sub>2</sub> surfaces: Principles, mechanisms, and selected results. *Chem. Rev.* **1995**, *95*, 735–758. [[CrossRef](#)]
8. Gupta, M.; Tripathi, M. A review of TiO<sub>2</sub> nanoparticles. *Chin. Sci. Bull.* **2011**, *56*, 1639–1657. [[CrossRef](#)]
9. Nakata, K.; Fujishima, A. TiO<sub>2</sub> Photocatalysis: Design and Applications. *J. Photochem. Photobiol. C Photochem. Rev.* **2012**, *13*, 169–189. [[CrossRef](#)]
10. Mukhtar, F.; Munawar, T.; Nadeem, M.S.; Batool, S.; Hasan, M.; Riaz, M.; Iqbal, F. Highly efficient tri-phase TiO<sub>2</sub>-Y<sub>2</sub>O<sub>3</sub>-V<sub>2</sub>O<sub>5</sub> nanocomposite: Structural, optical, photocatalyst, and antibacterial studies. *J. Nanostruct. Chem.* **2022**, *12*, 547–564. [[CrossRef](#)]
11. Bagheri, S.; Julkapli, N.M.; Hamid, S.B.A. Titanium Dioxide as a Catalyst Support in Heterogeneous Catalysis. *Sci. World J.* **2014**, *2014*, 727496. [[CrossRef](#)] [[PubMed](#)]
12. Kumar, O.P.; Shahzad, K.; Nazir, M.A.; Farooq, N.; Malik, M.; Ahmad Shah, S.S.; ur Rehman, A. Photo-Fenton activated C<sub>3</sub>N<sub>4</sub><sub>x</sub>/AgO<sub>y</sub>@Co<sub>1-x</sub>Bi<sub>0.1-y</sub>O<sub>7</sub> dual s-scheme heterojunction towards degradation of organic pollutants. *Opt. Mater.* **2022**, *126*, 112199. [[CrossRef](#)]
13. Tóth, Z.-R.; Debreczeni, D.; Gyulavani, T.; Szekely, I.; Todea, M.; Kovacs, G.; Focsa, M.; Magyari, K.; Baia, L.; Pap, Z.; et al. Rapid Synthesis Method of Ag<sub>3</sub>PO<sub>4</sub> as Reusable Photocatalytically Active Semiconductor. *Nanomaterials* **2023**, *13*, 89. [[CrossRef](#)] [[PubMed](#)]
14. Zaleska, A. Doped-TiO<sub>2</sub>: A Review. *Recent Pat. Eng.* **2008**, *2*, 157–164. [[CrossRef](#)]
15. Chen, L.; Rahme, K.; Holmes, J.D.; Morris, M.A.; Slater, N.K.H. Non-solvolytic synthesis of aqueous soluble TiO<sub>2</sub> nanoparticles and real-time dynamic measurements of the nanoparticle formation. *Nanoscale Res. Lett.* **2012**, *7*, 297–307. [[CrossRef](#)]
16. Srivastava, S.; Sinha, R.; Roy, D. Toxicological effects of malachite green—Review. *Aquat. Toxicol.* **2004**, *66*, 319–329. [[CrossRef](#)] [[PubMed](#)]
17. Fu, X.-Y.; Zhao, W.; Xiong, A.-S.; Tian, Y.-S.; Zhu, B.; Peng, R.-H.; Yao, Q.-H. Phytoremediation of triphenylmethane dyes by overexpressing a *Citrobacter* sp. triphenylmethane reductase in transgenic Arabidopsis. *Appl. Microbiol. Biotechnol.* **2013**, *97*, 1799–1806. [[CrossRef](#)]
18. Nazir, M.A.; Najam, T.; Bashir, M.S.; Javed, M.S.; Bashir, M.A.; Imran, M.; Azhar, U.; Shah, S.S.A.; Rehman, A.U. Kinetics, isothermal and mechanistic insight into the adsorption of eosin yellow and malachite green from water via tri-metallic layered double hydroxide nanosheets. *Korean J. Chem. Eng.* **2022**, *39*, 216–226. [[CrossRef](#)]
19. Raval, N.P.; Shah, P.U.; Shah, N.K. Malachite green “a cationic dye” and its removal from aqueous solution by adsorption. *Appl. Water Sci.* **2017**, *7*, 3407–3445. [[CrossRef](#)]
20. Franco, D.; Calabrese, G.; Guglielmino, S.P.P.; Conoci, S. Metal-Based Nanoparticles: Antibacterial Mechanisms and Biomedical Application. *Microorganisms* **2022**, *10*, 1778. [[CrossRef](#)]
21. Hamimed, S.; Chatti, A. Chapter 7: Photocatalytic metal bionanocomposites for biomedical applications. In *Bionanotechnology: Emerging Applications of Bionanomaterials*; Elsevier Inc.: Amsterdam, The Netherlands, 2022; pp. 227–258. [[CrossRef](#)]
22. Ishiguro, H.; Nakano, R.; Yao, Y.; Kajioaka, J.; Fujishima, A.; Sunada, K.; Minoshima, M.; Hashimoto, K.; Kubota, Y. Photocatalytic inactivation of bacteriophages by TiO<sub>2</sub>-coated glass plates under low-intensity, long-wavelength UV irradiation. *Photochem. Photobiol. Sci.* **2011**, *10*, 1825–1829. [[CrossRef](#)] [[PubMed](#)]
23. De Dicastillo, C.L.; Correa, M.G.; Martínez, F.B.; Streitt, C.; Galotto, M.J. Antimicrobial Effect of Titanium Dioxide Nanoparticles. In *Antimicrobial Resistance—A One Health Perspective*; IntechOpen: London, UK, 2020. [[CrossRef](#)]
24. Verdier, T.; Coutand, M.; Bertron, A.; Roques, C. Antibacterial activity of TiO<sub>2</sub> photocatalyst alone or in coatings on *E. coli*: The influence of methodological aspects. *Coatings* **2014**, *4*, 670–686. [[CrossRef](#)]
25. Vogel, W. *Chemistry of Glass*; Wiley-American Ceramic Society: Hoboken, NJ, USA, 1985.

26. Mukhtar, F.; Munawar, T.; Shahid Nadeem, M.; Naveedur Rehman, M.; Mahmood, K.; Batool, S.; Hasan, M.; Rehman, K.; Iqbal, F. Enhancement in carrier separation of ZnO-Ho<sub>2</sub>O<sub>3</sub>-Sm<sub>2</sub>O<sub>3</sub> heterostructured nanocomposite with rGO and PANI supported direct dual Z-scheme for antimicrobial inactivation and sunlight driven photocatalysis. *Adv. Powder Technol.* **2021**, *32*, 3770–3787. [[CrossRef](#)]
27. Stoyanova, A.; Bachvarova-Nedelcheva, A.; Iordanova, R.; Ivanova, N.; Hitkova, H.; Sredkova, M. Synthesis, photocatalytic and antibacterial properties of nanosized ZnTiO<sub>3</sub> powders obtained by different sol-gel methods. *Dig. J. Nanomater. Biostruct.* **2012**, *7*, 777–784.
28. Shalaby, A.; Bachvarova-Nedelcheva, A.; Iordanova, R.; Dimitriev, Y.; Stoyanova, A.; Hitkova, H.; Ivanova, N. Sol-gel synthesis and properties of nanocomposites in the Ag/TiO<sub>2</sub>/ZnO system. *J. Optoelectron. Adv. Mater.* **2015**, *17*, 248–256.
29. Bachvarova-Nedelcheva, A.; Iordanova, R.; Stoyanova, A.; Georgieva, N.; Angeova, T. Sol-gel synthesis of Se and Te containing TiO<sub>2</sub> nanocomposites with photocatalytic and antibacterial properties. *J. Optoelectron. Adv. Mater.* **2016**, *18*, 5–9.
30. Gegova, R.; Bachvarova-Nedelcheva, A.; Iordanova, R.; Dimitriev, Y. Synthesis and crystallization of gels in the TiO<sub>2</sub>-TeO<sub>2</sub>-ZnO system. *Bulg. Chem. Commun.* **2015**, *47*, 378–386.
31. Stoyanova, A.; Hitkova, H.; Bachvarova-Nedelcheva, A.; Iordanova, R.; Ivanova, N.; Sredkova, M. Synthesis and antibacterial activity of TiO<sub>2</sub>/ZnO nanocomposites prepared via nonhydrolytic route. *J. Chem. Technol. Metall.* **2013**, *48*, 154–161.
32. Weng, L.; Hodgson, S. Sol-gel processing of tellurite powder. *J. Mater. Sci.* **2001**, *36*, 4955–4959. [[CrossRef](#)]
33. Hodgson, S.N.B.; Weng, L. Processing and characterization of sol-gel glasses and powders in the system TeO<sub>2</sub>-TiO<sub>2</sub>. *J. Mater. Sci.* **2002**, *37*, 3059–3066. [[CrossRef](#)]
34. Hayakawa, T.; Koyama, H.; Nogami, M.; Thomas, P. Optical properties of TeO<sub>2</sub>-TiO<sub>2</sub> thin films doped with Eu<sup>3+</sup> ions fabricated by sol-gel processing. *J. Univ. Chem. Technol. Metall.* **2012**, *47*, 381–386.
35. Iordanova, R.; Bachvarova-Nedelcheva, A.; Gegova, R.; Dimitriev, Y. Sol-gel synthesis of composite powders in the TiO<sub>2</sub>-TeO<sub>2</sub>-SeO<sub>2</sub> system. *J. Sol-Gel Sci. Technol.* **2016**, *79*, 12–28. [[CrossRef](#)]
36. St I, Y.; Bachvarova-Nedelcheva, A.D.; Iordanova, R.S. Influence of ethylene glycol on the hydrolysis-condensation behavior of Ti(IV) butoxide. *Bulg. Chem. Commun. Spec. Issue A* **2017**, *49*, 265–270.
37. Lecomte, A.; Bamiere, F.; Coste, S.; Thomas Ph Champarnaud-Mesjard, J.C. Sol-gel processing of TeO<sub>2</sub> thin films from citric acid stabilized tellurium isopropoxide precursor. *J. Eur. Ceram. Soc.* **2007**, *27*, 1151–1158. [[CrossRef](#)]
38. Saylikan, F.; Asilturk, M.; Saylikan, H.; Onal, Y.; Akarsu, M.; Aprac, E. Characterization of TiO<sub>2</sub> synthesized in alcohol by a sol-gel process: The effects of annealing temperature and acid catalyst. *Turk. J. Chem.* **2005**, *29*, 697–706.
39. Madarász, J.; Brăileanu, A.; Crișan, M.; Pokol, G. Comprehensive evolved gas analysis (EGA) of amorphous precursors for s-doped titania by in situ TG-FTIR and TG/DTA-MS in air: Part 2. Precursor from thiourea and titanium(IV)-n-butoxide. *J. Anal. Appl. Pyrolysis* **2009**, *85*, 549–556. [[CrossRef](#)]
40. Doeuff, S.; Henry, M.; Sanchez, C.; Livage, J. Hydrolysis of titanium alkoxides: Modification of the molecular precursor by acetic acid. *J. Non-Cryst. Solids* **1987**, *89*, 206–216. [[CrossRef](#)]
41. Wei, H.Y.; Lin, J.; Huang, W.H.; Feng, Z.B.; Li, D.W. Preparation of TeO<sub>2</sub> based thin films by nonhydrolytic sol-gel process. *Mater. Sci. Eng. B* **2009**, *164*, 51–59. [[CrossRef](#)]
42. Kato, K.; Tsuge, A.; Niihara, K. Microstructure and Crystallographic Orientation of Anatase Coatings Produced from Chemically Modified Titanium Tetraisopropoxide. *J. Am. Ceram. Soc.* **1996**, *79*, 1483–1488. [[CrossRef](#)]
43. Barboux-Doeuff, S.; Sanchez, C. Synthesis and characterization of titanium oxide-based gels synthesized from acetate modified titanium butoxide precursors. *Mater. Res. Bull.* **1994**, *29*, 1–13. [[CrossRef](#)]
44. Uzunova-Bujnova, M.; Dimitrov, D.; Radev, D.; Bojinova, A.; Todorovsky, D. Effect of the mechanoactivation on the structure, sorption and photocatalytic properties of titanium dioxide. *Mater. Chem. Phys.* **2008**, *110*, 291–298. [[CrossRef](#)]
45. Murashkevich, N.; Lavitskaya, A.S.; Barannikova, T.I.; Zharskii, I.M. Infrared absorption spectra and structure of TiO<sub>2</sub>. *J. Appl. Spectrosc.* **2008**, *75*, 730–734. [[CrossRef](#)]
46. Bachvarova-Nedelcheva, A.; Iordanova, R.; Kostov, K.L.; Yordanov St Ganev, V. Structure and properties of a Non-Traditional Glass Containing TeO<sub>2</sub>, SeO<sub>2</sub> and MoO<sub>3</sub>. *Opt. Mater.* **2012**, *34*, 1781–1787. [[CrossRef](#)]
47. Dimitriev, Y.; Dimitrov, V.; Arnaudov, M. IR spectra and structures of tellurite glasses. *J. Mater. Sci.* **1983**, *18*, 1353–1358. [[CrossRef](#)]
48. Arnaudov, M.; Dimitrov, V.; Dimitriev, Y. Infrared-spectral investigation of tellurites. *Mater. Res. Bull.* **1982**, *17*, 1121–1129. [[CrossRef](#)]
49. Iordanova, R.; Gegova, R.; Bachvarova-Nedelcheva, A.; Dimitriev, Y. Sol-gel synthesis of composites in the ternary TiO<sub>2</sub>-TeO<sub>2</sub>-B<sub>2</sub>O<sub>3</sub> system. *Phys. Chem. Glasses Eur. J. Glass Sci. Technol. B* **2015**, *56*, 128–138. [[CrossRef](#)]
50. Barlier, V.; Bounor-Legare, V.; Boiteux, G.; Davenas, J. Hydrolysis-condensation reactions of titanium alkoxides in thin films: A study of the steric hindrance effect by X-ray photoelectron spectroscopy. *Appl. Surf. Sci.* **2008**, *254*, 5408–5412. [[CrossRef](#)]
51. Nagaveni, K.; Hegde, M.S.; Ravishankar, N.; Subbanna, G.N.; Madras, G. Synthesis and Structure of Nanocrystalline TiO<sub>2</sub> with Lower Band Gap Showing High Photocatalytic Activity. *Langmuir* **2004**, *20*, 2900–2907. [[CrossRef](#)]
52. Ngyen Vi Nu Hoai Beydoun, D.; Amal, R. Photocatalytic reduction of selenite and selenate using TiO<sub>2</sub> photocatalyst. *J. Photochem. Photobiol. A Chem.* **2005**, *171*, 113–120.
53. Meng, Z.D.; Zhu, L.; Ullah, K.; Ye, S.; Oh, W.-C. Detection of oxygen species generated by WO<sub>3</sub> modification fullerene/TiO<sub>2</sub> in the degradation of 1,5-diphenyl carbazide. *Mater. Res. Bull.* **2014**, *56*, 45–53. [[CrossRef](#)]

54. Weng, L.; Hodgson, N.B. Multicomponent tellurite thin film materials with high refractive index. *Opt. Mater.* **2002**, *19*, 313–317. [[CrossRef](#)]
55. Saidin, S.; Jumat, M.A.; Amin, N.A.A.M.; Al-Hammadi, A.S.S. Organic and inorganic antibacterial approaches in combating bacterial infection for biomedical application. *Mater. Sci. Eng. C* **2021**, *118*, 111382. [[CrossRef](#)] [[PubMed](#)]
56. Bachvarova-Nedelcheva, A.; Yordanov St Iordanova, R.; Stambolova, I.; Stoyanova, A.; Georgieva, N.; Nemska, V. The influence of Nd and Sm on the structure and properties of sol-gel derived TiO<sub>2</sub> powders. *Molecules* **2021**, *26*, 3824. [[CrossRef](#)] [[PubMed](#)]
57. Nakano, R.; Hara, M.; Ishiguro, H.; Yao, Y.; Ochiai, T.; Nakata, K.; Murakami, T.; Kajioaka, J.; Sunada, K.; Hashimoto, K.; et al. Broad spectrum microbicidal activity of photocatalysis by TiO<sub>2</sub>. *Catalysts* **2013**, *3*, 310–323. [[CrossRef](#)]
58. Godoy-Gallardo, M.; Eckhard, U.; Delgado, L.M.; de Roo Puente, Y.J.; Hoyos-Nogués, M.; Gil, F.J.; Perez, R.A. Antibacterial Approaches in Tissue Engineering Using Metal Ions and Nanoparticles: From Mechanisms to Applications. *Bioact. Mater.* **2021**, *6*, 4470–4490. [[CrossRef](#)]
59. Kumar, K.; Porkodi, K.; Rocha, F. Langmuir-Hinshelwood kinetics—A theoretical study. *Catal. Comm.* **2008**, *9*, 82–84. [[CrossRef](#)]
60. Chan, C.M.N.; Ng, A.M.C.; Fung, M.K.; Cheng, H.S.; Guo, M.Y.; Djurišić, A.B.; Leung, F.C.C.; Chan, W.K. Antibacterial and photocatalytic activities of TiO<sub>2</sub> nanotubes. *J. Exp. Nanosci.* **2013**, *8*, 859–867. [[CrossRef](#)]
61. Girish, S.; Gomathi Devi, L. Review on Modified TiO<sub>2</sub> Photocatalysis under UV/Visible Light: Selected Results and Related Mechanisms on Interfacial Charge Carrier Transfer Dynamics. *J. Phys. Chem. A* **2011**, *115*, 13211–13241.
62. Bachvarova-Nedelcheva, A.; Iordanova, R.; Georgieva, N.; Nemska, V. Preparation, characterization and antibacterial assessment of sol-gel derived TiO<sub>2</sub>/TeO<sub>2</sub>/ZnO powders. *J. Chem. Technol. Metall.* **2022**, *57*, 589–597.
63. Kanno, Y.; Hihara, T.; Watanabe, T.; Katoh, K. *Low Sulfate Generation Diesel Oxidation Catalyst*; SAE Technical Paper, 2004-01-1427; SAE: Warrendale, PA, USA, 2004.
64. Hirata, H.; Hachisuka, I.; Ikeda, Y.; Tsuji, S.; Matsumoto, S. NO<sub>x</sub> storage-reduction three-way catalyst with improved sulfur tolerance. *Top. Catal.* **2001**, *16*, 145–149. [[CrossRef](#)]
65. Weng, L.; Hodgson, S.; Bao, X.; Sagoe-Crentsil, K. Achieving controllable sol-gel processing of tellurite glasses through the use of Te(VI) precursors. *Mater. Sci. Eng.* **2004**, *B107*, 89–93. [[CrossRef](#)]
66. Hodgson, S.; Weng, L. Chemical and sol-gel processing of tellurite glasses for optoelectronics. *J. Mater. Sci. Mater. Electron.* **2006**, *17*, 723–733. [[CrossRef](#)]
67. Weng, L.; Hodgson, S. Sol-gel processing of tellurite materials from tellurium ethoxide precursor. *Mater. Sci. Eng. B* **2001**, *87*, 77–82. [[CrossRef](#)]
68. Shalaby, A.; Dimitriev, Y.; Iordanova, R.; Bachvarova-Nedelcheva, A.; Iliev, T. Modified sol-gel synthesis of submicron powders in the system ZnO-TiO<sub>2</sub>. *J. Univ. Chem. Technol. Metall.* **2011**, *46*, 137–142.
69. Hagen, J. *Industrial Catalysis a Practical Approach*; WileyVCH GmbH: Weinheim, Germany, 2006; pp. 227–228.
70. Valgas, C.; de Souza, S.M.; Smania, E.F.A., Jr. Screening methods to determine antibacterial activity of natural products. *Braz. J. Microbiol.* **2007**, *38*, 369–380. [[CrossRef](#)]

**Disclaimer/Publisher's Note:** The statements, opinions and data contained in all publications are solely those of the individual author(s) and contributor(s) and not of MDPI and/or the editor(s). MDPI and/or the editor(s) disclaim responsibility for any injury to people or property resulting from any ideas, methods, instructions or products referred to in the content.